Journal of Environmental Radioactivity 297 (2026) 108027

Contents lists available at ScienceDirect

Journal of Environmental Radioactivity

journal homepage: www.elsevier.com/locate/jenr

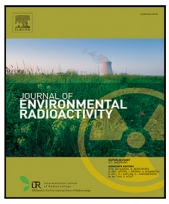

Radioactivity behavior in hydrothermal volcanic systems: Preliminary *in situ* investigations at high and low gas flux degassing areas

Giordano Bufi [a], Silvia Massaro [a,b], Francesco Giordano [c], Pierfrancesco Dellino [a], Silvia Raino' [c,*], Alessandro Aiuppa [d], Giulio Bini [e], Stefano Caliro [e], Davide Cerasole [c], Antonio Costa [b], Fabio Dioguardi [a], Danilo Elenterio [c], Simone Lentini [a], Francesca Romana Pantaleo [c,f], Francesco Rufino [e], Giancarlo Tamburello [b], Angelo Vitale [d], Georges Vougioukalakis [g], Antonio Zaccaro [c], Roberto Sulpizio [a,b]

[a] *Università degli Studi di Bari Aldo Moro Dipartimento di Scienze della Terra e Geoambientali, Italy*
[b] *Istituto Nazionale di Geofisica e Vulcanologia, Sezione di Bologna, Italy*
[c] *Università degli Studi di Bari Dipartimento Interateneo di Fisica Michelangelo Merlin, Italy*
[d] *Università di Palermo Dipartimento di Scienze della Terra e del Mare, Italy*
[e] *Istituto Nazionale di Geofisica e Vulcanologia Osservatorio Vesuviano, Italy*
[f] *Politecnico di Bari, Italy*
[g] *Hellenic Survey of Geology & Mineral Exploration, Greece*

ARTICLE INFO

Keywords:
Gamma-ray spectroscopy
Volcanic degassing
Pisciarelli fumarolic field
Campi Flegrei
Stephanos crater
Nisyros

ABSTRACT

Long-term investigations at numerous active volcanic systems worldwide have demonstrated that environmental radionuclide measurements in volcanic plumes provide valuable insights into degassing processes, yielding important constraints on magmatic activity timescales and the depth of magmatic reservoirs. In this study, we introduce a novel methodological framework for the environmental characterization of airborne radioactivity, aimed at quantifying the coupled atmospheric transport of radionuclides and gas species (e.g., CO_2 and H_2S) in active volcanic environments. The approach integrates *in situ* gamma-ray spectroscopy with geochemical measurements of air concentrations, enabling a direct comparison between radiometric signals and volcanic gas transport. The method was applied to two distinct active volcanic sites: the Pisciarelli fumarolic field (Campi Flegrei caldera, Italy), characterized by a sustained gas flux, and the Stephanos crater (Nisyros Island, Greece) where passive gas emissions are comparatively low. Gamma-ray detection acquired at multiple heights above ground (ranging from 40 to 180 cm) allowed the assessment of vertical variations in radioactivity levels and volcanic gas concentrations from both diffuse and fumarolic sources, even under very low-emission conditions. Our results show a clear coupling between CO_2 concentration and gamma radiation, demonstrating that volcanic gases act as carriers of radon and its progeny, significantly modifying the vertical distribution of radioactivity. These findings provide the first direct field evidence of height-dependent radionuclide transport driven by gas fluxes and establishes a new framework for real-time environmental radioactivity monitoring in volcanic areas.

1. Introduction

In recent decades, the study of natural radioactivity has attracted increasing attention (MacKenzie, 2000). Monitoring natural radioactivity is crucial not only for assessing potential health risks (Shahbazi-Gahrouei et al., 2013), but also for understanding the behavior and distribution of radioactive sources in the environment (Al-Khawlany et al., 2018). The main contribution to natural radiation arises from radionuclides in rocks, soil, and water, such as Uranium (^{238}U), Thorium (^{232}Th), and their decay products, including Radon. The latter is particularly important, as it accounts for most of the dose from natural sources of ionizing radiation and is widely present in the Earth's crust (Ambrosino et al., 2020a,b). Despite the challenges associated with sampling and measurement, noble gas radionuclides provide unique insights into active hydrothermal systems, particularly in terms of fluid residence times and geochemical evolution, e.g., (Yokochi et al., 2021; Fischer and Chiodini, 2015; Iovine et al., 2022). Radon, in particular, is widely used to trace natural processes such as seismotectonic (Igarashi et al., 1995) and volcanic activity (Le Cloarec and

* Corresponding author.
E-mail address: silvia.raino@uniba.it (S. Raino').
[1] https://www.amptek.com/internal-products/obsolete-products/gamma-rad5-gamma-ray-detection-system

https://doi.org/10.1016/j.jenvrad.2026.108027
Received 10 July 2025; Received in revised form 26 April 2026; Accepted 30 April 2026
Available online 15 May 2026
0265-931X/© 2026 The Authors. Published by Elsevier Ltd. This is an open access article under the CC BY license (http://creativecommons.org/licenses/by/4.0/).

Pennisi, 2002; Koike et al., 2014; Giammanco et al., 2023), as its concentration is strongly controlled by rock dilation (Sakoda et al., 2011), magmatic degassing, and advective hydrothermal fluid flow through faults, e.g., (Ambrosino et al., 2020a; Singh et al., 2017; Planinić et al., 2001). Although influenced by multiple environmental factors, the Radon signal can provide both local and remote information, especially when continuously recorded at a given site (Sabbarese et al., 2020; Terray et al., 2020). However, the relative contribution of the ^{238}U and ^{232}Th series in volcanic environments, as well as the interaction of Radon with other gas species in the gaseous phase, remains an open issue. In general, when the collisional Van der Waals (VdW) radius of the carrier gas is comparable to that of radionuclides, the latter can be transported into the atmosphere. In volcanic environments, the most common gases (i.e., H_2O, CO_2, H_2S, SO_2, CH_4) may interact with the two main Radon radioisotopes:^{222}Rn (half-life of 3.82 days), produced by ^{226}Ra decay in the ^{238}U series, and ^{220}Rn (half-life of 55.6 s), produced from ^{224}Ra in the ^{232}Th series (Ambrosino et al., 2020a; Hwa Oh and Kim, 2015). Given their markedly different half-lives, a shift in the ^{222}Rn/^{220}Rn ratio toward higher ^{220}Rn concentrations suggests that the carrier gas pathway is sufficiently short to allow detection of ^{220}Rn radionuclides (Ambrosino et al., 2021). This can be considered a first-order indicator of gas source depth (shallow vs. deep), which is particularly relevant for volcanic surveillance, e.g., at Mt. Etna (Giammanco et al., 2007, 2023). Therefore, simultaneous monitoring of radionuclide activity and gas concentrations is essential, while disentangling the contributions from soil-emitted radiation and gaseous sources. Recent studies on uranium-thorium-derived Radon production (^{222}Rn/^{220}Rn) have mainly focused on soil contributions, e.g., (Li et al., 2022; D'Incecco et al., 2021), using gamma-ray detectors such as RaMonA or RAD7, e.g., (Ambrosino et al., 2020a; Hwa Oh and Kim, 2015; Mollo et al., 2021), to distinguish between slow and fast gas transport and between shallow and deep radiogenic sources, e.g., (Etiope and Lombardi, 1995; Mollo et al., 2021). According to Bini et al. (2020), gas measured in volcanic soils can be interpreted as a mixture of two components: (1) shallow gas production (low ^{222}Rn/^{220}Rn) in undisturbed soil, and (2) deep gas production (high ^{222}Rn/^{220}Rn) efficiently transported to the surface by carrier gases such as CO_2 (Gauthier and Condomines, 1999; Cigolini et al., 2013; Miklyaev et al., 2022). Here, we present a novel *in situ* methodological approach for radioactivity measurements that integrates ground-level gamma-ray spectroscopy with passive gas dispersion analysis, specifically designed to isolate the gaseous contribution from the total radiation signal. The approach is applied to two active hydrothermal volcanic systems characterized by contrasting diffusive CO_2 fluxes: the La Solfatara-Pisciarelli system (Campi Flegrei, Italy), which exhibits relatively high emissions (ca. 4000-5000 t d^{-1}) (Chiodini et al., 2021), and the Stephanos crater (Nisyros Island, Greece), with significantly lower emissions (17-25 t d^{-1}) (Bini et al., 2019; Massaro et al., 2024). Two gas surveys were conducted between January and July 2024 to simultaneously measure gamma radiation and gas concentrations at different atmospheric heights, using the portable spectrometer GAMMA-RAD5 (AMPTEK[1]) and the multi-component gas analyzer MultiGAS (Aiuppa et al., 2005). In this study, we focus on spatial variability, while temporal trends will be addressed in future work. Although the two investigated sites are closed systems (i.e. no magma exposed to the surface), the method proved robust and highlighted differences in their gamma-ray spectra response. Moreover, the average radionuclide count rate (cps) measured at different heights correlates well with gas concentrations at the same levels, supporting the role of CO_2 as a carrier of ^{222}Rn,^{220}Rn, and their progeny (see Fig. 1).

1.1. Pisciarelli fumarolic field (La Solfatara crater, Italy)

The Pisciarelli fumarolic field is located on the eastern slope of La Solfatara crater (Campi Flegrei caldera; Fig. 2a) within the so called Diffuse Degassing Structure area (DDS) (Chiodini et al., 2001; Cardellini et al., 2017) which spans approximately 1.4 km^2 and is characterized by numerous fault structures e.g., (Capuano et al., 2013; Cardellini et al., 2017). Estimates of total CO_2 emissions from the DDS indicate an increase from about 1000 t d^{-1} in 2008-2010 to 3000-4000 t d^{-1} in 2019-2020. At Pisciarelli, a primary vent releases overpressurized gases from a mud pool. In addition, several smaller fumaroles are also present in the area. Recent flux measurements (Aiuppa et al., 2013; Tamburello et al., 2019) indicate a fumarolic CO_2 emission rate of approximately 600 t d^{-1}.

Biagi et al. (2022) carried out a gas survey in 2020 showing the occurrence of anomalously high CO_2 and H_2S concentrations at the near-surface level, clearly associated to hydrothermal discharges (Chiodini et al., 2021). Time series of atmospheric CO_2 concentrations recorded by the Osservatorio Vesuviano geochemical station (FLUXOV8), show a significant increasing trend over time since 2013. Recent data indicate that this trend has become significantly more pronounced with an average concentration of 4500 ppm recorded in April 2025.[2]

1.2. Stephanos crater (Nisyros island, Greece)

Stephanos crater is located in the Lakki Plain (Nisyros island, Greece; Fig. 2b), a hydrothermal volcanic area affected by NE trending active faults as also revealed by alignment of fumarolic vents (Dietrich and Lagios, 2017). The fumarolic gas discharges show exit temperatures between 96 and 100 °C, close to the boiling point of water at sea level. These emissions are composed primarily of water vapor (H_2O_v) followed by CO_2 and H_2S, while N_2, H_2, CH_4, CO, Ar, and He are minor components. The absence of strongly acid gases indicates that the fumarolic effluents are generated from a boiling hydrothermal reservoir rather than from direct magma degassing (Chiodini et al., 1993).

Over the past 20 years, the total soil CO_2 emission from the degassing area of ca. 2.2 km^2 has ranged from 81.6±6.8 t d^{-1} during 1999–2001 to 100.6±7.9 t d^{-1} in 2018 (Bini et al., 2019).

Bini et al. (2020) applied a multi-parametric approach within the caldera to differentiate between deep and shallow gas sources. This involved measuring soil CO_2 flux, carbon isotopic composition, soil temperatures and ^{222}Rn/^{220}Rn activity using the RAD7 radon detector at 80 cm depth in the ground. Their analysis revealed that seasonal variations in biogenic CO_2 production significantly affect the total CO_2 output and that the deep soil CO_2 fluxes spatially correlate with both soil temperatures and ^{222}Rn/^{220}Rn ratios. Recently, Massaro et al. (2024) used the averaged H_2O flux from five fumaroles of the Stephanos crater and the averaged H_2S/H_2O weight ratio of ~0.0049 to get a representative averaged H_2S flux for a single fumarole of approximately 2.4 10^{-4} t d^{-1} during April–June 2023.

2. Materials and methods

During the 2024 field surveys, total gamma radiation (cps) and CO_2 concentration (ppm) were simultaneously measured across the investigated areas at the Pisciarelli fumarolic field and the Stephanos crater. Gamma radiation was measured using a portable gamma spectrometer (AMPTEK GAMMA-RAD5), equipped with a single NaI(Tl) scintillation crystal detector coupled to a photomultiplier and a digital pulse processor (DP5-AMPTEK). The system provides an energy resolution of 6.5% at 662 keV. Calibration and gain stabilization were automatically performed by the instrument control software (DPPMCA), which uses the natural background ^{40}K peak as an internal reference. This approach compensates for thermal and temporal drifts without requiring an internal radioactive source. Such spectrometers are commonly used for laboratory measurements or static long-duration acquisitions aimed

[2] https://www.ov.ingv.it/index.php/monitoraggio-e-infrastrutture/bollettini-tutti/bollett-mensili-cf/anno-2025-3/1773-bollettino-mensile-campi-flegrei-2025-04/file; last access: 22-04-2026

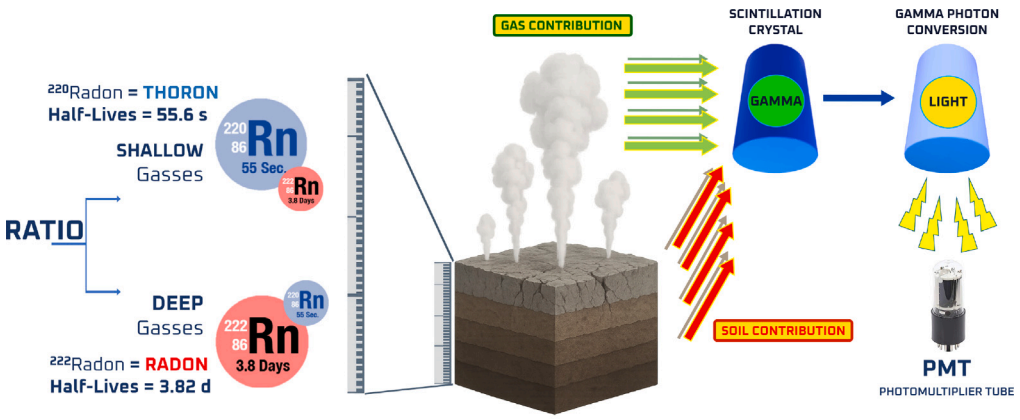

Fig. 1. Sketch of the contribution provided by the ^{222}Rn and ^{220}Rn through rocks and gas plume which can be detected by the gamma spectrometer GAMMA-RAD5 (AMPTEK).

at radionuclide quantification in soils (Melquiades et al., 2024), as well as for testing the shielding properties of materials (Rani et al., 2020).

The spectrometer was mounted on a camera tripod via a custom-made adapter, allowing measurements at different atmospheric heights (0, 40, 100, 140, and 180 cm).

Gas concentrations were measured using a lightweight (<3 kg) portable multi-component gas analyzer (MultiGAS; Aiuppa et al. (2005)), positioned on the ground near the sampling tube and in close proximity to the spectrometer. At the Pisciarelli vent, gas concentrations were recorded at 1 Hz using an Arduino data logger connected to two CO_2 sensors with different measurement ranges: a Licor 830 (0–20000 ppm; 2%) and a supplemental Cozir GSS Sprint-IR 20% (0–200000 ppm; 20%), used to extend the measurement range under direct plume exposure. At the Stephanos crater, measurements were continuously acquired at 1 Hz using a Campbell Scientific CR6 data logger connected to a CO_2 sensor (non-dispersive infrared spectroscopy; Edinburgh Sensors NG Gas Card, detection range 0–3000 ppm; 3%) and an H_2S electrochemical sensor (CiTiceL T3H, detection range 0–200 ppm). All sensors were connected through a pneumatic circuit of silicone tubing, with ambient air drawn at a flow rate of 1.4 L min^{-1} by a diaphragm pump. The exact position of each sampling point was recorded using a synchronized GPS. Radiometric and gas measurements were time-synchronized to ensure direct comparison between atmospheric composition and gamma response at each sampling point.

To ensure full daily coverage of the study areas, simultaneous measurements of gamma radiation and gas concentrations were performed with a fixed acquisition time of one minute per point. This acquisition time represented a compromise between counting statistics, spatial coverage, and the need to resolve rapid short-term variations in volcanic gas flux and atmospheric dispersion during field operations. This relatively short interval minimizes the influence of rapidly changing weather conditions, which can significantly affect gas dispersion and transport direction. Wind data were acquired concurrently with gas sampling: at the Pisciarelli fumarolic field using two permanent weather stations, and at the Stephanos crater using a commercial anemometer.[3]

3. Results

This section presents the results of the data acquisitions conducted at both investigated sites, which reflect their distinct geological settings and operational constraints. At Pisciarelli, the rugged topography and the high hazard level associated with ongoing seismic unrest within the Campi Flegrei caldera limited the duration of field activities. Consequently, the implementation of a systematic measurement grid was not feasible. Data collection was therefore restricted to three discrete sampling points, with vertical profiles limited to two heights: 0 cm (ground level) and 140 cm. In contrast, the relatively flat morphology of the Stephanos crater, combined with low-risk conditions, allowed for a more comprehensive and flexible survey design. This setting enabled the implementation of a regular sampling grid and the acquisition of vertical profiles up to 180 cm above ground level.

These constraints led us to prioritize the spatial mapping of radioactivity, while detailed spectral analysis and the investigation of radionuclide temporal trends will be addressed in future dedicated campaigns.

3.1. Measurements at Pisciarelli fumarolic field (high flux degassing area)

At the Pisciarelli site, three measurement points (P1, P2, and P3; Fig. 3a) were selected across the degassing area:

- P1 is located near the site entrance, on a topographic ridge, and is exposed to strong wind variability;
- P2 lies in proximity to the main plume;
- P3 is located outside the plume, where gas flux is mainly diffusive and lower. Vegetation in this area marks a distinct morphological boundary of the mud pool system.

Fig. 3b shows the average CO_2 concentrations (ppm) versus total gamma radiation rates (cps), measured at ground level (solid dots) and at 140 cm height (open dots). The total gamma rate was calculated by summing counts across all spectral channels (excluding the pedestal) and normalizing by the acquisition time. The mean of two consecutive measurements was then computed to verify data stability and reproducibility.

CO_2 concentrations were obtained by averaging instantaneous readings collected simultaneously with gamma measurements at the same atmospheric levels. Measurements were repeated twice, in June (black) and July (red) 2024 (Fig. 3b), to assess reproducibility under different degassing conditions. At P1 and P3 (both outside the main plume), gas flux was predominantly diffusive. Average CO_2 concentrations remained close to background levels (slightly above 420 ppm) and decreased with height. A similar trend was observed in gamma-ray rates, which decreased from 1900 to 1800 cps at P1 and from ca. 1620 to ca. 1540 cps at P3. In contrast, at P2, located downwind of the main plume, significantly higher CO_2 concentrations were recorded, resulting from wind conditions that funneled the plume directly into the MultiGAS inlet. The large and rapid CO_2 fluctuations, occurring

[3] Testo-405i Thermal Anemometer; https://www.testo.com/it-IT/testo-405i/p/0560-1405

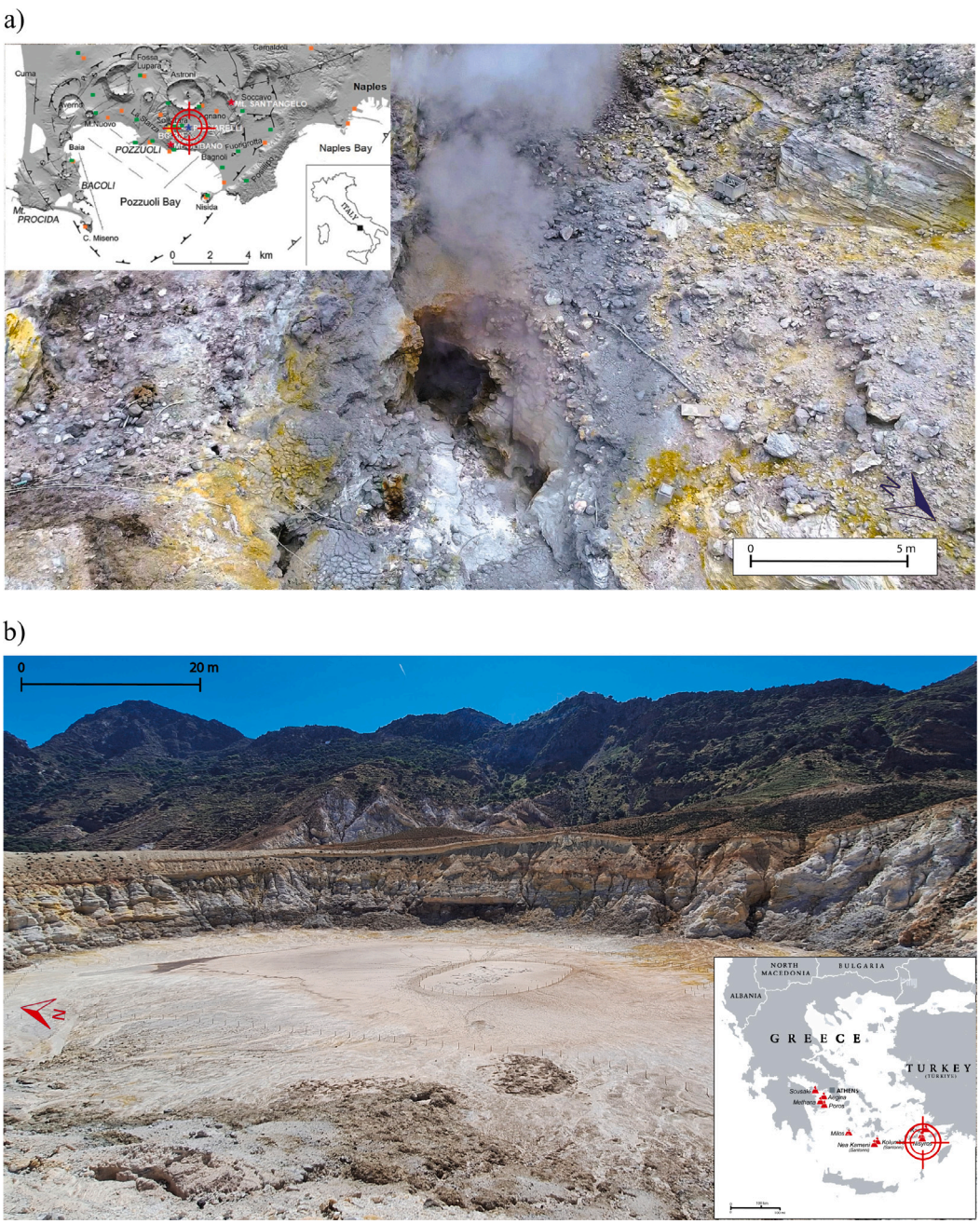

Fig. 2. Location of the investigated sites: (a) Campi Flegrei caldera (south Italy) showing the La Solfatara crater (red circle) and (b) Nisyros island (Greece). Photos of the active plume at Pisciarelli and Stephanos crater taken during the gas surveys are shown. (For interpretation of the references to color in this figure legend, the reader is referred to the web version of this article.)

over timescales as short as one minute, reflect the high gas flux and complicate the representation of variability at this point. Some time series are characterized by short-lived spikes lasting 5–10 s within the 60 s acquisition interval. While the mean value remains representative of overall CO_2 conditions, the standard deviation is strongly influenced by the coexistence of background levels (420–450 ppm) and transient peaks, thus reflecting signal intermittency rather than effective gas exposure relevant to transport processes. To address this, error bars were estimated by weighting the contribution of high-concentration spikes according to their relative duration (~10% of the acquisition time), providing a more representative measure of the effective gas-phase contribution. Despite this variability, the gamma-ray rate at P2 remained relatively stable, around 2000 cps (July 2024) and 1900 cps (June 2024), at both measurement heights. At 140 cm, the carrier effect of the gas appears to partly offset the natural decrease in gamma radiation typically observed with increasing distance from the radiogenic source (i.e., ground-level rocks). To further investigate the relationship between CO_2 concentration and radionuclide transport, a Spearman rank correlation analysis was performed under the assumption of an exponential behavior. Only P1 and P2 were considered representative of the system, while P3 was treated as a background reference. The analyzed variables were: (i) the relative difference between tGR measured at 140 cm and at ground level, normalized to the maximum ground value, and (ii) the average CO_2 concentration between the two heights. The latter choice avoids potential bias that could arise from using concentration differences. The resulting correlation coefficient ($\rho = -0.8$) indicates a strong inverse monotonic relationship, whereby increasing CO_2 concentrations correspond to a progressive reduction in

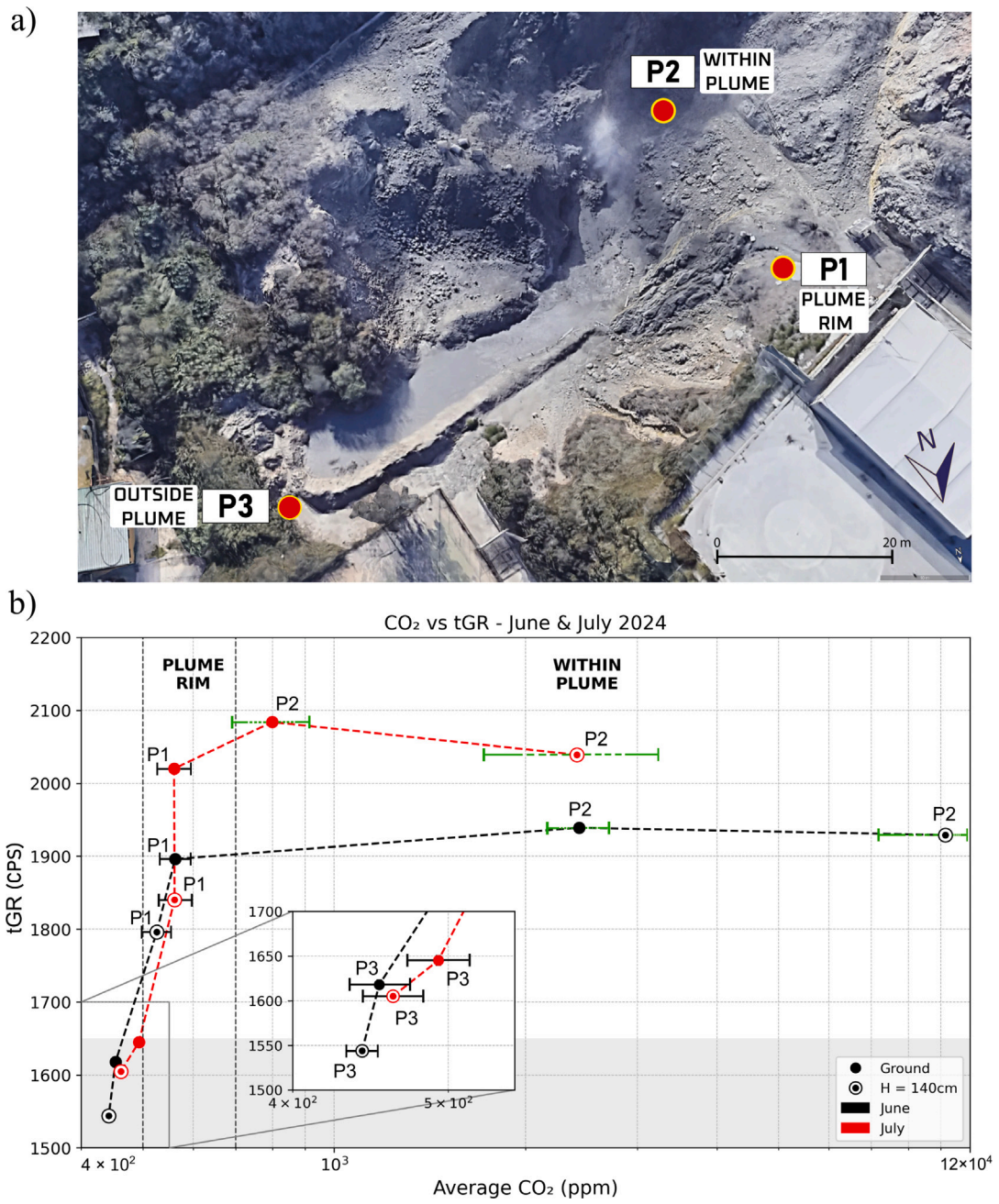

Fig. 3. (a) Satellite image of the Pisciarelli fumarolic field showing the measurement points P1, P2, P3 (from Google Earth); (b) Total gamma rate versus the average CO_2 concentrations measured at ground level (full circle) and at 140 cm height (dotted circle) during 26 June (red line) and 26 July 2024 (black line). The averaged wind speed and direction measured from 9 am to 5 pm from the gas station V07 (INGV-Osservatorio Vesuviano) was 2.7 m/s, 188° *N* (26 June 2024) and 2.25 m/s, 178° *N* (26 July 2024). The gray band represent the background range of the gamma-ray rates measured within the investigated area. (For interpretation of the references to color in this figure legend, the reader is referred to the web version of this article.)

the vertical *tGR* gradient. This supports the hypothesis that higher gas concentrations enhance radionuclide transport. However, the observations also suggest the presence of a threshold effect: although CO_2 is a well-known carrier of radionuclides, further increases in gas flux do not necessarily lead to enhanced radionuclide transport, contrary to what might be expected. Table 1 summarizes the average CO_2 concentrations and total gamma rates, along with their associated uncertainties and variability, for both campaigns.

3.2. Measurements at stephanos crater (low flux degassing area)

At Stephanos crater, twelve measurement points were selected, covering nearly the entire crater area (Fig. 4a), where approximately 70 fumaroles were active along the crater rim at the time of the survey (Massaro et al., 2024). For each point, five measurements of total gamma radiation and CO_2 and H_2S concentrations were performed at ground level and at heights of 40, 100, 140, and 180 cm above ground. Given the relatively low gas emissions of this system, we assume that the soil contribution to radioactivity dominates over the fumarolic component, with only a limited fraction of radionuclides transported into the atmosphere. To test this hypothesis, Fig. 4b shows three representative points of the grid, reporting average CO_2 concentrations (ppm) versus total gamma radiation rates (cps), measured at ground level (circles), 100 cm (squares), and 180 cm (triangles). Table 2 summarizes the average CO_2 concentrations and total gamma rates, together with

Table 1
Averaged CO_2 (ppm) and total gamma rate (tGR; cps) measurements and their standard deviations σ at (a–c) ground and (b–d) 140 cm height during the June and July 2024 surveys at the Pisciarelli fumarolic field.

(a) Ground Scan (0 cm) – June 2024				
Point	Average CO_2 (ppm)	σ-CO_2	tGR (cps)	σ-tGR
P1	5.6×10^2	0.9×10^2	1896	8
P2	2.4×10^3	3.4×10^3	1939	8
P3	4.5×10^2	0.2×10^2	1618	7
(b) Height Scan (140 cm) – June 2024				
Point	Average CO_2 (ppm)	σ-CO_2	tGR (cps)	σ-tGR
P1	5.3×10^2	0.7×10^2	1796	8
P2	9.0×10^3	17.0×10^3	1929	8
P3	4.42×10^2	0.07×10^2	1544	7
(c) Ground Scan (0 cm) – July 2024				
Point	Average CO_2 (ppm)	σ-CO_2	tGR (cps)	σ-tGR
P1	5.6×10^2	0.7×10^2	2020	8
P2	8.0×10^2	12.0×10^2	2084	8
P3	4.9×10^2	0.2×10^2	1645	7
(d) Height Scan (140 cm) – July 2024				
Point	Average CO_2 (ppm)	σ-CO_2	tGR (cps)	σ-tGR
P1	5.6×10^2	1.8×10^2	1840	8
P2	2.4×10^3	7.8×10^3	2039	8
P3	4.6×10^2	0.2×10^2	1605	7

Table 2
Averaged CO_2 (ppm) and total gamma rate (tGR; cps) measurements and their standard deviations σ at (a) ground, (b) 100 cm height, and (c) 180 cm height taken at points 1A, 2B and 2E within the Stephanos crater during April 2024.

(a) Ground Scan (0 cm)				
Point	Average CO_2 (ppm)	σ-CO_2	tGR (cps)	σ-tGR
1A	4.78×10^2	0.12×10^2	1745	5
2B	4.82×10^2	0.07×10^2	1575	5
2E	5.41×10^2	0.14×10^2	1136	4
(b) Height Scan (100 cm)				
Point	Average CO_2 (ppm)	σ-CO_2	tGR (cps)	σ-tGR
1A	4.77×10^2	0.12×10^2	1623	5
2B	4.82×10^2	0.91×10^2	1543	5
2E	4.89×10^2	0.12×10^2	1134	4
(c) Height Scan (180 cm)				
Point	Average CO_2 (ppm)	σ-CO_2	tGR (cps)	σ-tGR
1A	4.56×10^2	0.11×10^2	1488	5
2B	4.78×10^2	0.08×10^2	1454	5
2E	5.35×10^2	0.12×10^2	1138	4

their associated standard deviations. As expected, the overall radiation trend decreases from non-fumarolic points (1A and 2B) to the fumarolic point (2E), consistent with a higher degree of fracturing and lower soil density in fumarolic areas. A Spearman rank correlation was also computed between the relative tGR difference and the average CO_2 concentration, considering the three measurement points shown in Fig. 4. The resulting coefficient ($\rho = -1$) indicates a perfect inverse monotonic relationship. Although this result is strongly influenced by the limited number of data points and should therefore be interpreted with caution, the observed trend is consistent with the reduction of the vertical tGR gradient with increasing CO_2 concentration, similarly to the Pisciarelli case. The observed relationship between CO_2 and tGR motivated a more direct assessment of the potential contribution of radionuclides in the gas phase. This was addressed by analyzing the vertical variation of total gamma radiation, with measurements at each grid point normalized to their respective mean values using the Z-score method (Johnson et al., 2002). The underlying hypothesis is that, in areas influenced by fumarolic activity, the dependence of gamma radiation on height is reduced compared to locations where the soil contribution dominates.

Fig. 5 presents maps of normalized total gamma radiation, as well as average CO_2 and H_2S concentrations, linearly interpolated over the grid at ground level and at 180 cm height. Wind speed was measured over the same time interval as gas and radioactivity data and is reported here for reference only. At ground level (Fig. 5a), the eastâ–west sector of the crater exhibits the highest normalized gamma radiation values, whereas the outer rim areas show comparatively lower values, despite the presence of localized fumarolic activity. In contrast, at 180 cm height (Fig. 5b), the highest normalized gamma radiation values are observed in two distinct areas: a well-defined sector along the inner southeastern rim, and a southwestern sector associated with higher CO_2 and H_2S emissions. These observations indicate that, even under low-flux conditions, fumarolic activity can promote radionuclide transport into the atmosphere. At higher elevations, the carrier effect of CO_2 appears to partially counterbalance the natural decrease in gamma radiation with increasing distance from the source.

3.3. Integral gamma-ray spectra at the two degassing sites

As a complementary analysis, representative full gamma-ray spectra acquired at the two investigated sites were compared to assess overall spectral features and detector performance under field conditions (Fig. 6). The selected spectra correspond to measurement points where average radioactivity and gas concentrations at ground level exceeded background values. All spectra were normalized to a common acquisition time of 600 s to allow direct comparison. The spectra acquired at Pisciarelli and Stephanos show differences in total intensity and spectral shape, indicating distinct geological backgrounds and degassing conditions (Fig. 6a). Spectra are shown both as raw data (thin lines) and in rebinned form (thick lines). Rebinning reduces the number of energy channels from 8192 (set by the 13-bit ADC) to 2048, improving statistical robustness and computational efficiency for peak fitting. Variations in spectral shape and peak intensity reflect differences in the geological background of the two sites and may be related to their degassing activity. Distinct photopeaks are visible in both spectra, confirming the capability of the detector to resolve characteristic natural gamma emissions during field measurements. Only a qualitative spectral comparison is presented in (Fig. 6a). Gaussian fits of the ^{40}K photopeak at 1460 keV are reported in Figs. 6b–c for the two representative spectra, used to evaluate the peak identification capability and instrumental energy resolution. The signal (N_S) and background (N_B) counts were obtained by integrating the fitted components over an energy interval centered on the Gaussian mean and extending to $\pm 3\sigma$. The peak significance S was then calculated as N_S/σ_{S+B}, where σ_{S+B} includes both statistical and fitting uncertainties. It is worth noting that these results confirm the suitability of the adopted system for rapid in situ gamma-ray investigations in active volcanic environments. Table 3 summarizes the corresponding count statistics, peak significance, and spectral resolution. Fig. 7 presents additional comparisons of spectra acquired at ground level and at 140 cm height for representative points at both sites, further highlighting the capability of the system to detect spectral differences related to site conditions and measurement height.

4. Discussion and conclusions

4.1. Capabilities of the gamma radiation detection at volcanic sites

In this study, we introduce a methodology designed to simultaneously capture the *in situ* full gamma radiation spectrum and gas concentrations at different heights above ground. This approach extends beyond conventional methods, which are typically limited to long-term identification of specific radionuclides, by providing a combined evaluation of gas transport processes in two active volcanic systems. These systems exhibit contrasting degassing regimes and are affected by safety constraints that limit data acquisition activities. In such environments, advective fluid transport through permeable soils can carry radon radionuclides over considerable distances, e.g., (Neri et al., 2016). However, in the absence of preferential pathways such as

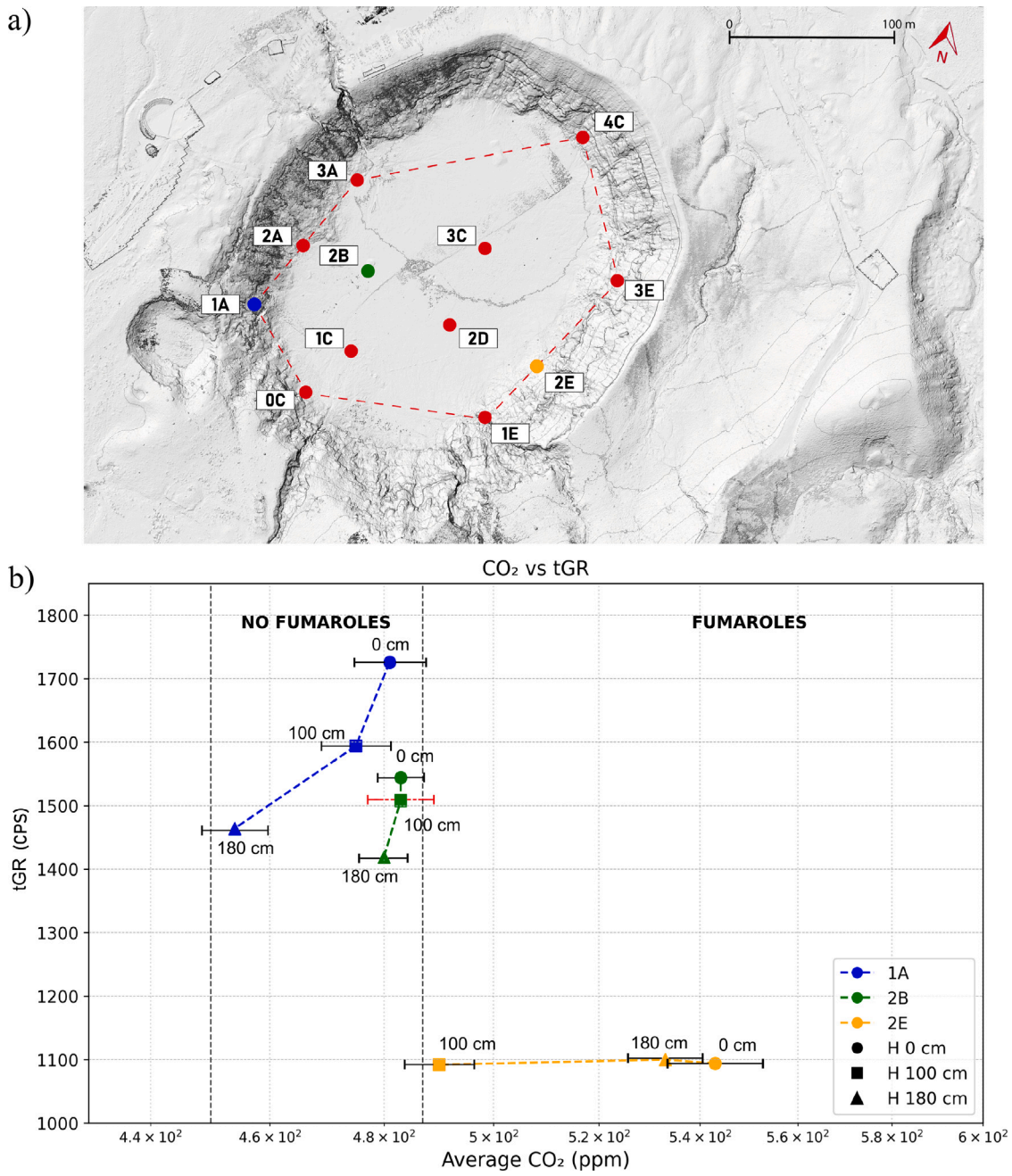

Fig. 4. (a) Digital Elevation Model of the Stephanos crater (1 m resolution) showing the measuring points. (b) Total gamma rate versus the average CO_2 concentrations measured at ground level (full circle), at 100 cm height (square) and at 140 cm height (triangle).

fractures or faults, the $^{222}Rn/^{220}Rn$ activity mainly reflects shallow gas production from Uâ–Th-bearing minerals in the rockâ–soil matrix (Bini et al., 2020). At Pisciarelli, we infer a stronger contribution from deep-seated fluids compared to the Stephanos crater, although emissions at both sites remain predominantly hydrothermal. Gamma radiation levels at Pisciarelli are slightly higher, likely due to differences in lithology and more efficient gas transport into the atmosphere. At both sites, vertical variations in gamma radiation follow the expected decrease with increasing distance from radiogenic soil and rocks. However, fumarolic plumes can partially counterbalance this trend at higher elevations. At Stephanos, where gas flux is relatively low, normalization of gamma radiation measurements was necessary to better resolve this effect (Fig. 5b). Natural radioactivity has long been used to investigate the origin and evolution of magmatic activity, although several limitations remain. The short half-lives of the main radionuclides (3.8 days for ^{222}Rn and 55 s for ^{220}Rn) restrict their effectiveness as tracers, as their migration is strongly influenced by rock permeability, structural features, and environmental factors such as atmospheric pressure, temperature, and precipitation (Mollo et al., 2018; Amestoy et al., 2021). Moreover, radon anomalies do not always directly correlate with magma-related crustal sources, requiring long-term monitoring and integration with other geochemical and geophysical datasets for reliable interpretation, e.g., (Laiolo et al., 2016). In volcanic settings, high CO_2 fluxes through permeable lithologies can dilute or suppress the radiogenic signal, particularly the $^{222}Rn/^{220}Rn$ ratio, by overwhelming

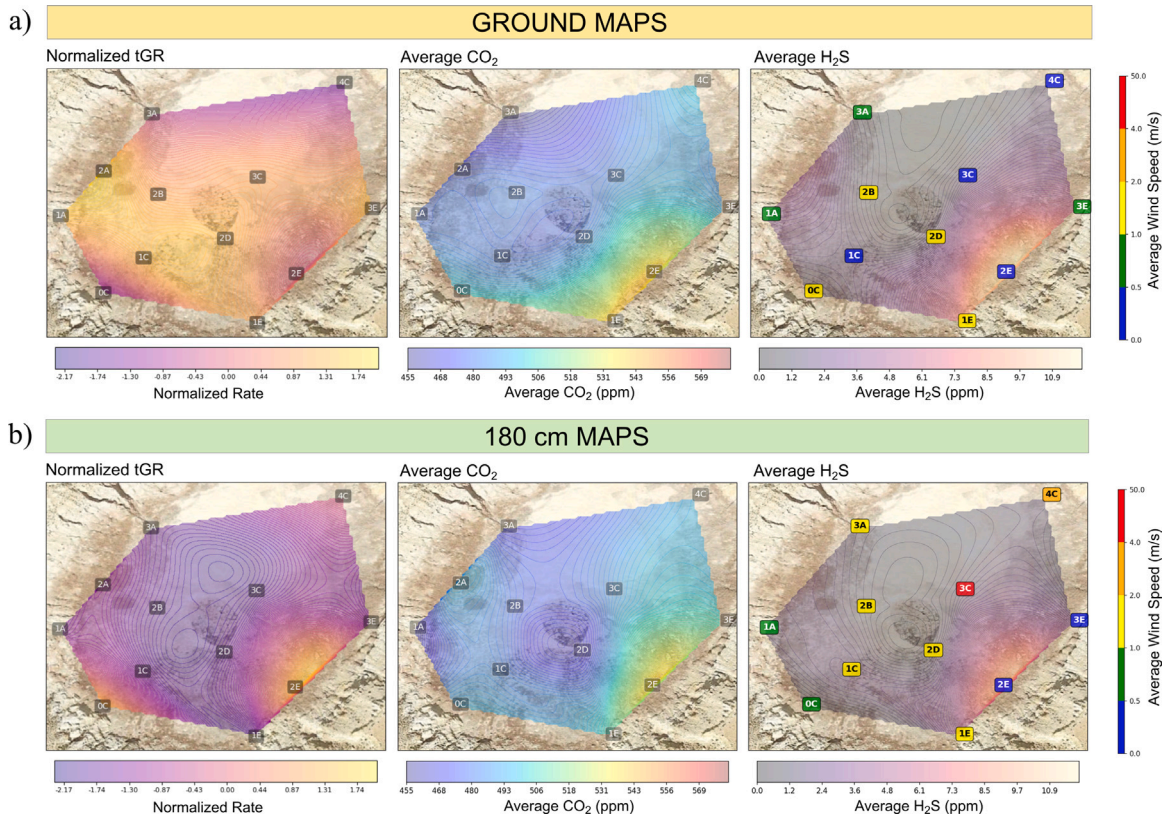

Fig. 5. Maps at (a) ground level and (b) 180 cm height of the averaged normalized total gamma rate (tGR, cps) (left), CO_2 (mid) and H_2S (right) concentration (ppm). The averaged wind speed at each measurement point is reported with colored flags indicating the intensity (from blue, low intensity, to red, high intensity). The maps were obtained using a linear interpolation method. (For interpretation of the references to color in this figure legend, the reader is referred to the web version of this article.)

Table 3
Spectral peak fitting parameters for the selected points at Pisciarelli (P1, P2) and Stephanos crater (1A, 2E) at ground and 140 cm height.
Definitions:
A_p = Peak area; σ_p = Peak area error; A_{bkg} = Background area; σ_{bkg} = Background area error; A_{tot} = Total area; σ_{tot} = Total area error; μ = Mean of the Gaussian distribution representing the most probable energy of the photopeak under analysis.
* Significance = A_p/σ_{tot}.
** Resolution = σ/μ.

Point name	A_p	σ_p	A_{bkg}	σ_{bkg}	A_{tot}	σ_{tot}	Sig.*	Res.**
1A_140 cm	2.55×10^3	1.96×10^2	1.05×10^4	1.87×10^2	1.31×10^4	1.11×10^2	2.31×10^1	3.50×10^{-2}
1A_ground	3.02×10^3	2.08×10^2	1.16×10^4	2.04×10^2	1.46×10^4	1.13×10^2	2.67×10^1	3.20×10^{-2}
2E_140 cm	3.57×10^3	1.45×10^2	6.23×10^3	1.24×10^2	9.80×10^3	9.62×10^1	3.72×10^1	3.30×10^{-2}
2E_ground	4.20×10^3	1.49×10^2	6.81×10^3	1.22×10^2	1.10×10^4	1.02×10^2	4.11×10^1	3.40×10^{-2}
P1_140 cm	6.69×10^3	1.12×10^2	3.03×10^3	5.86×10^1	9.72×10^3	9.76×10^1	6.85×10^1	2.30×10^{-2}
P1_ground	1.57×10^4	1.80×10^2	7.58×10^3	1.02×10^2	2.33×10^4	1.51×10^2	1.04×10^2	2.40×10^{-2}
P2_140 cm	7.78×10^3	1.40×10^2	5.24×10^3	8.75×10^1	1.30×10^4	1.13×10^2	6.89×10^1	2.90×10^{-2}
P2_ground	3.85×10^3	9.36×10^1	2.14×10^3	5.68×10^1	5.99×10^3	7.67×10^1	5.02×10^1	2.80×10^{-2}

shallow contributions. Studies at Mt Etna (Sicily, Italy) and along active flank faults have shown a progressive dilution of $^{222}Rn/^{220}Rn$ with increasing CO_2 flux (Giammanco et al., 2007, 2009). A similar mechanism may explain the behavior observed at Pisciarelli (P2), where the gamma radiation remains nearly constant despite increasing CO_2 concentrations (Fig. 3b). Laboratory experiments by Mollo et al. (2021) on zeolitized tuff under variable CO_2 fluxes showed that enhancement of the ^{220}Rn signal is most effective at relatively low CO_2 fluxes, where the carrier effect dominates. At higher fluxes, however, radionuclide transport by advection is counterbalanced by strong dilution within the carrier gas. Additionally, gas migration through lithologies with different petrophysical properties can produce coupling or decoupling between $^{222}Rn/^{220}Rn$ and CO_2 emissions (Etiope and Lombardi, 1995).

4.2. Present-day limitations and next methodological advancements

Several low-cost instruments have been developed for use in harsh volcanic environments, but these passive systems are generally limited to long-term integrated measurements of alpha-emitting radionuclides such as ^{222}Rn and ^{220}Rn (Laiolo et al., 2016; Terray et al., 2020). Because alpha particles have a very short penetration range, their detection requires close proximity or direct contact, limiting

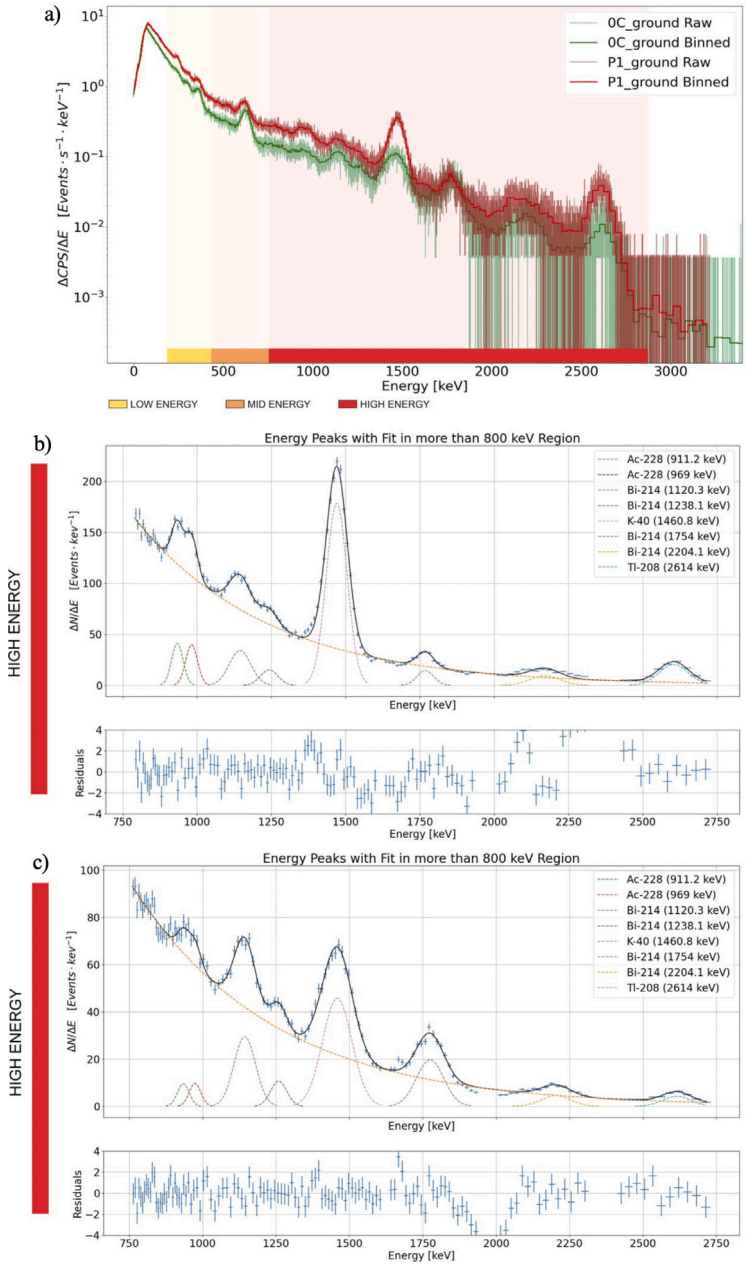

Fig. 6. (a) Integral gamma-ray spectra as a function of energy, normalized to a common time interval of 600 s to enable consistent comparison between the two ground measurement locations at Pisciarelli fumarolic field (P1, red curve) and Stephanos crater (0C, green curve). (b) and (c) Gaussian fits of the ^{40}K photopeak at 1460 keV for the two representative spectra used to evaluate the peak identification capability and instrumental energy resolution. (For interpretation of the references to color in this figure legend, the reader is referred to the web version of this article.)

spatial resolution and real-time monitoring. In contrast, gamma-ray spectrometry allows continuous and remote detection of multiple radionuclides, providing higher temporal resolution and enabling the identification of isotopic signatures in dynamic degassing environments, e.g., (Knoll, 2010). Amestoy et al. (2021) investigated the influence of environmental factors on airborne gamma-ray spectrometry (K, U, Th), showing that atmospheric ^{222}Rn concentrations vary on daily and seasonal timescales due to changes in soil exhalation rates driven by humidity and meteorological conditions. Although relevant, a detailed assessment of these effects is beyond the scope of this study.

The relatively short acquisition times used in this study (1-600 s), imposed by logistical and safety constraints, represent another limitation. Future applications could benefit from longer measurements and the use of airborne platforms such as drones would improve data quality and enable access to remote or hazardous areas, including active vents where manual acquisition is often not feasible (Cigolini et al., 2013; Inguaggiato et al., 2013).

By comparing sites with different degassing regimes, this study shows that real-time monitoring of environmental radioactivity, combined with simultaneous gas measurements, can improve the identification of site-specific radionuclide signatures and their atmospheric transport (e.g., ^{222}Rn/^{220}Rn). Although radionuclide ratios were not directly quantified due to the limited number of measurements and relatively short acquisition times, this work provides a baseline for an integrated approach tailored to the geological characteristics of the investigated systems. Such an approach may offer a robust framework

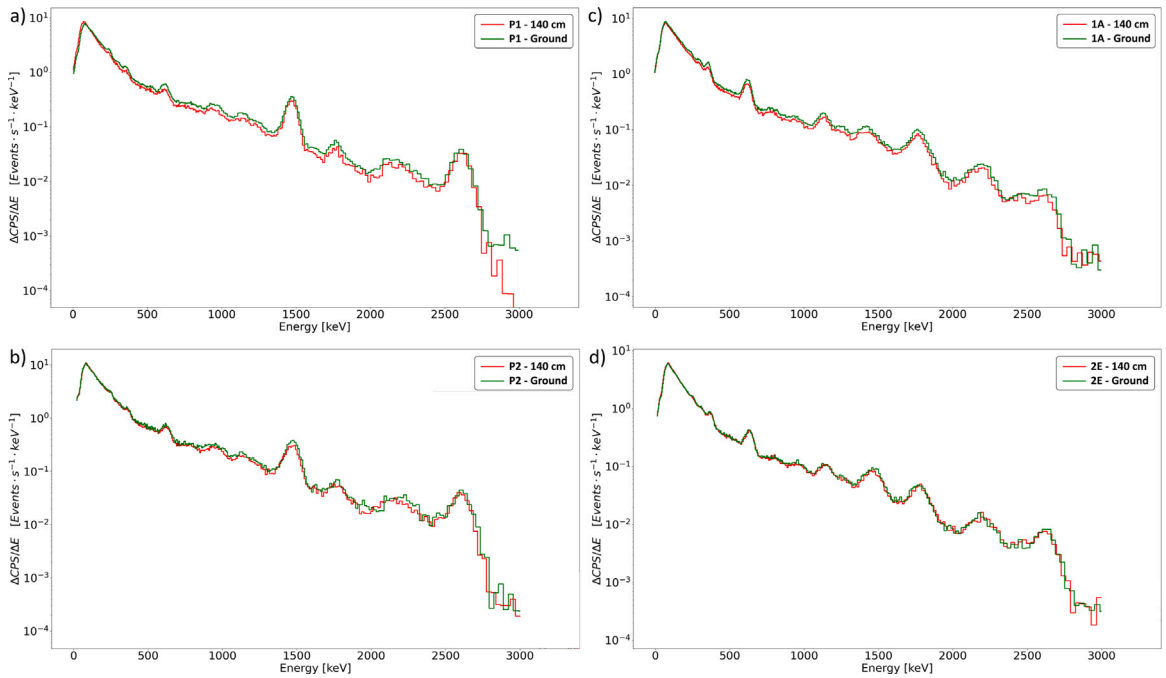

Fig. 7. Comparison of spectra at ground level and 140 cm height for two selected points of the investigated sites. For Pisciarelli fumarolic field, (a) P1 (outside plume) and (b) P2 (within plume). For Stephanos crater, (c) 1A (far from fumaroles) and (d) 2E (close to fumaroles).

for distinguishing between shallow and deep degassing sources, a task often complicated by temporal variability in conventional methods. For this reason, more accurate quantification of radionuclide ratios will be the focus of future investigations.

CRediT authorship contribution statement

Giordano Bufi: Writing – review & editing, Visualization, Software, Methodology, Investigation, Formal analysis, Data curation, Conceptualization. **Silvia Massaro:** Writing – review & editing, Writing – original draft, Validation, Supervision, Methodology, Investigation, Formal analysis, Data curation, Conceptualization. **Francesco Giordano:** Validation, Supervision, Resources, Project administration, Methodology, Conceptualization. **Pierfrancesco Dellino:** Validation, Supervision, Resources, Project administration, Conceptualization. **Silvia Raino':** Writing – review & editing, Validation, Supervision, Methodology. **Alessandro Aiuppa:** Writing – review & editing, Resources, Methodology. **Giulio Bini:** Writing – review & editing, Validation, Resources. **Stefano Caliro:** Validation, Resources, Methodology, Investigation, Data curation. **Davide Cerasole:** Investigation, Formal analysis, Data curation. **Antonio Costa:** Writing – review & editing, Validation, Methodology, Investigation, Formal analysis. **Fabio Dioguardi:** Writing – review & editing, Investigation. **Danilo Elenterio:** Software, Formal analysis. **Simone Lentini:** Resources, Investigation, Data curation. **Francesca Romana Pantaleo:** Validation. **Francesco Rufino:** Writing – review & editing, Resources, Methodology, Data curation. **Giancarlo Tamburello:** Writing – review & editing, Resources, Investigation, Data curation. **Angelo Vitale:** Resources, Methodology, Investigation, Data curation. **Georges Vougioukalakis:** Writing – review & editing, Validation. **Antonio Zaccaro:** Software, Formal analysis, Data curation. **Roberto Sulpizio:** Validation, Supervision, Project administration, Methodology, Investigation, Funding acquisition, Conceptualization.

Declaration of Generative AI and AI-assisted technologies in the writing process

During the preparation of this work the authors used ChatGPT (OpenAI) in order to improve the writing quality and enhance the fluency of the text. After using this tool, the authors reviewed and edited the content as needed and take full responsibility for the content of the published article.

Declaration of competing interest

The authors declare that they have no known competing financial interests or personal relationships that could have appeared to influence the work reported in this paper.

Acknowledgements

PD, FD, SM, RS, GB acknowledge the RETURN Extended Partnership and received funding from the European Union Next-GenerationEU (National Recovery and Resilience Plan–NRRP, Mission 4, Component 2, Investment 1.3–D.D. 1243 2/8/2022, PE0000005). AC, SM, SC and FR thank the INGV-CPV (Centro di Pericolosità Vulcanica) Project 2023-2025.

Appendix

See Fig. A.1.

Data availability

Data will be made available on request.

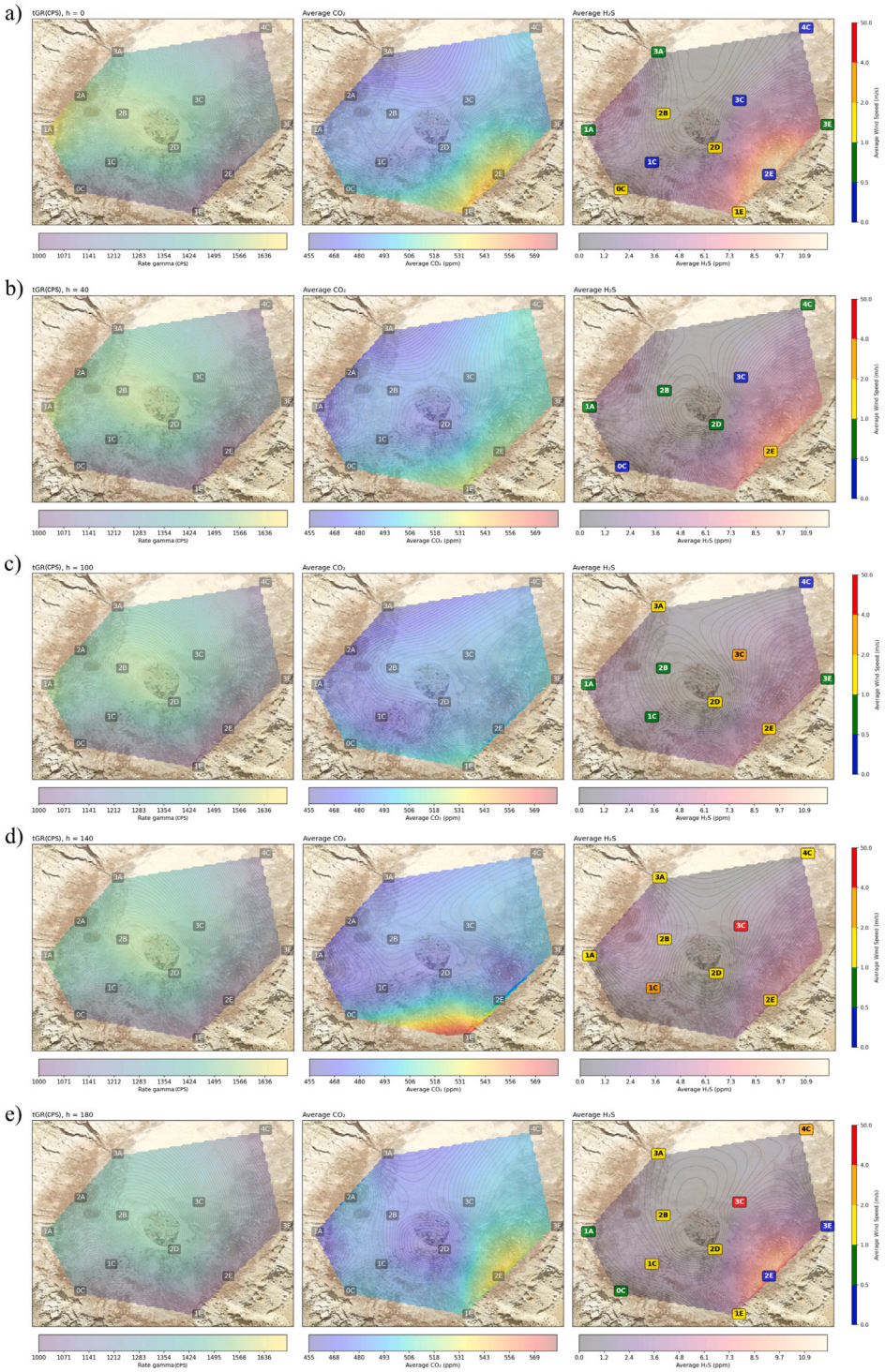

Fig. A.1. Detail of the integral gamma radiation spectra acquired for 600 s showing the main peaks at low, medium and high energy at Stephanos crater (0C - ground).

References

Aiuppa, A., Federico, C., Giudice, G., Gurrieri, S., 2005. Chemical mapping of a fumarolic field: la fossa crater, Vulcano Island (Aeolian Islands, Italy). Geophys. Res. Lett. 32 (13).

Aiuppa, A., Tamburello, G., Di Napoli, R., Cardellini, C., Chiodini, G., Giudice, G., Grassa, F., Pedone, M., 2013. First observations of the fumarolic gas output from a restless caldera: Implications for the current period of unrest (2005–2013) at Campi Flegrei. Geochem. Geophys. Geosyst. 14 (10), 4153–4169.

Al-Khawlany, A.H., Khan, A., Pathan, J., 2018. Review on studies in natural background radiation. Radiat. Prot. Environ. 41 (4), 215–222.

Ambrosino, F., Sabbarese, C., Giudicepietro, F., De Cesare, W., Pugliese, M., Roca, V., 2021. Study of surface emissions of 220rn (thoron) at two sites in the campi flegrei caldera (Italy) during volcanic unrest in the period 2011–2017. Appl. Sci. 11 (13), 5809.

Ambrosino, F., Sabbarese, C., Roca, V., Giudicepietro, F., Chiodini, G., 2020a. Analysis of 7-years radon time series at Campi Flegrei area (naples, Italy) using artificial neural network method. Appl. Radiat. Isot. 163, 109239.

Ambrosino, F., Sabbarese, C., Roca, V., Giudicepietro, F., De Cesare, W., 2020b. Connection between 222rn emission and geophysical-geochemical parameters recorded during the volcanic unrest at campi flegrei caldera (2011–2017). Appl. Radiat. Isot. 166, 109385.

Amestoy, J., Meslin, P.Y., Richon, P., Delpuech, A., Derrien, S., Raynal, H., Pique, É., Baratoux, D., Chotard, P., Van Beek, P., et al., 2021. Effects of environmental factors on the monitoring of environmental radioactivity by airborne gamma-ray spectrometry. J. Environ. Radioact. 237, 106695.

Biagi, R., Tassi, F., Caliro, S., Capecchiacci, F., Venturi, S., 2022. Impact on air quality of carbon and sulfur volatile compounds emitted from hydrothermal discharges: The case study of pisciarelli (campi flegrei, south Italy). Chemosphere 297, 134166.

Bini, G., Chiodini, G., Cardellini, C., Vougioukalakis, G.E., Bachmann, O., 2019. Diffuse emission of CO2 and convective heat release at nisyros caldera (Greece). J. Volcanol. Geotherm. Res. 376, 44–53.

Bini, G., Chiodini, G., Lucchetti, C., Moschini, P., Caliro, S., Mollo, S., Selva, J., Tuccimei, P., Galli, G., Bachmann, O., 2020. Deep versus shallow sources of CO2 and Rn from a multi-parametric approach: the case of the nisyros caldera (aegean arc, Greece). Sci. Rep. 10 (1), 13782.

Capuano, P., Russo, G., Civetta, L., Orsi, G., D'Antonio, M., Moretti, R., 2013. The active portion of the campi flegrei caldera structure imaged by 3-D inversion of gravity data. Geochem. Geophys. Geosyst. 14 (10), 4681–4697.

Cardellini, C., Chiodini, G., Frondini, F., Avino, R., Bagnato, E., Caliro, S., Lelli, M., Rosiello, A., 2017. Monitoring diffuse volcanic degassing during volcanic unrests: the case of Campi Flegrei (Italy). Sci. Rep. 7 (1), 6757.

Chiodini, G., Caliro, S., Avino, R., Bini, G., Giudicepietro, F., De Cesare, W., Ricciolino, P., Aiuppa, A., Cardellini, C., Petrillo, Z., et al., 2021. Hydrothermal pressure-temperature control on CO2 emissions and seismicity at campi flegrei (Italy). J. Volcanol. Geotherm. Res. 414, 107245.

Chiodini, G., Cioni, R., Leonis, C., Marini, L., Raco, B., 1993. Fluid geochemistry of nisyros island, dodecanese, Greece. J. Volcanol. Geotherm. Res. 56 (1–2), 95–112.

Chiodini, G., Frondini, F., Cardellini, C., Granieri, D., Marini, L., Ventura, G., 2001. CO2 degassing and energy release at solfatara volcano, campi flegrei, Italy. J. Geophys. Res.: Solid Earth 106 (B8), 16213–16221.

Cigolini, C., Laiolo, M., Ulivieri, G., Coppola, D., Ripepe, M., 2013. Radon mapping, automatic measurements and extremely high 222Rn emissions during the 2002–2007 eruptive scenarios at stromboli volcano. J. Volcanol. Geotherm. Res. 264, 49–65.

Dietrich, V.J., Lagios, E., 2017. Nisyros Volcano: the Kos-Yali-Nisyros Volcanic Field. Springer.

D'Incecco, S., Petraki, E., Priniotakis, G., Papoutsidakis, M., Yannakopoulos, P., Nikolopoulos, D., 2021. CO2 and radon emissions as precursors of seismic activity. Earth Syst. Environ. 5 (3), 655–666.

Etiope, G., Lombardi, S., 1995. Evidence for radon transport by carrier gas through faulted clays in Italy. J. Radioanal. Nucl. Chem. 193 (2), 291–300.

Fischer, T.P., Chiodini, G., 2015. Volcanic, magmatic and hydrothermal gases. In: The Encyclopedia of Volcanoes. Elsevier, pp. 779–797.

Gauthier, P.J., Condomines, M., 1999. 210Pb–226Ra radioactive disequilibria in recent lavas and radon degassing: inferences on the magma chamber dynamics at stromboli and merapi volcanoes. Earth Planet. Sci. Lett. 172 (1–2), 111–126.

Giammanco, S., Bonfanti, P., Neri, M., 2023. Radon on Mt. Etna (Italy): a useful tracer of geodynamic processes and a potential health hazard to populations. Front. Earth Sci. 11, 1176051.

Giammanco, S., Immè, G., Mangano, G., Morelli, D., Neri, M., 2009. Comparison between different methodologies for detecting radon in soil along an active fault: The case of the pernicana fault system, Mt. Etna (Italy). Appl. Radiat. Isot. 67 (1), 178–185.

Giammanco, S., Parello, F., Gambardella, B., Schifano, R., Pizzullo, S., Galante, G., 2007. Focused and diffuse effluxes of CO2 from mud volcanoes and mofettes south of Mt. Etna (Italy). J. Volcanol. Geotherm. Res. 165 (1–2), 46–63.

Hwa Oh, Y., Kim, G., 2015. A radon-thoron isotope pair as a reliable earthquake precursor. Sci. Rep. 5 (1), 13084.

Igarashi, G., Saeki, S., Takahata, N., Sumikawa, K., Tasaka, S., Sasaki, Y., Takahashi, M., Sano, Y., 1995. Ground-water radon anomaly before the Kobe earthquake in Japan. Science 269 (5220), 60–61.

Inguaggiato, S., Paz, M.J., Mazot, A., Granados, H.D., Inguaggiato, C., Vita, F., 2013. CO2 output discharged from Stromboli island (Italy). Chem. Geol. 339, 52–60.

Iovine, R.S., Piochi, M., Avino, R., Cuoco, E., Minopoli, C., Santi, A., Caliro, S., Piersanti, A., Galli, G., 2022. Radon (222rn) levels in thermal waters of the geothermally active campi flegrei volcanic caldera (southern Italy): A framework study using a RAD7 radon detector. J. Volcanol. Geotherm. Res. 431, 107641.

Johnson, R.A., Wichern, D.W., et al., 2002. Applied Multivariate Statistical Analysis. Prentice hall Upper Saddle River, NJ.

Knoll, G.F., 2010. Radiation Detection and Measurement. John Wiley & Sons.

Koike, K., Yoshinaga, T., Ueyama, T., Asaue, H., 2014. Increased radon-222 in soil gas because of cumulative seismicity at active faults. Earth, Planets Space 66, 1–9.

Laiolo, M., Ranaldi, M., Tarchini, L., Carapezza, M., Coppola, D., Ricci, T., Cigolini, C., 2016. The effects of environmental parameters on diffuse degassing at stromboli volcano: Insights from joint monitoring of soil CO2 flux and radon activity. J. Volcanol. Geotherm. Res. 315, 65–78.

Le Cloarec, M., Pennisi, M., 2002. Radionuclide behavior in high-temperature gases from Satsuma Iwojima volcano, Japan. Earth, Planets Space 54 (3), 287–294.

Li, P., Sun, Q., Geng, J., Shi, Q., Hu, J., Tang, S., 2022. A study on the differences in radon exhalation of different lithologies at various depths and the factors influencing its distribution in northern Shaanxi, China. Sci. Total Environ. 849, 157935.

MacKenzie, A.B., 2000. Environmental radioactivity: experience from the 20th century—trends and issues for the 21st century. Sci. Total Environ. 249 (1–3), 313–329.

Massaro, S., Tamburello, G., Bini, G., Costa, A., Stocchi, M., Tassi, F., Biagi, R., Vaselli, O., Chiodini, G., Dioguardi, F., et al., 2024. Quantification of volcanic degassing and analysis of uncertainties using numerical modeling: the case of stephanos crater (nisyros island, Greece). Bull. Volcanol. 86 (12), 95.

Melquiades, F.L., Bastos, R.O., Rampim, L., Sandrino, I.I., Rodriguez, D.G., Parreira, P.S., 2024. Thorium and uranium rapid quantification in soil with portable X-ray fluorescence. Soil Sci. Am. J. 88 (2), 557–564.

Miklyaev, P.S., Petrova, T.B., Shchitov, D.V., Sidyakin, P.A., Murzabekov, M.A., Tsebro, D.N., Marennyy, A.M., Nefedov, N.A., Gavriliev, S.G., 2022. Radon transport in permeable geological environments. Sci. Total Environ. 852, 158382.

Mollo, S., Moschini, P., Galli, G., Tuccimei, P., Lucchetti, C., Iezzi, G., Scarlato, P., 2021. Carrier and dilution effects of CO2 on thoron emissions from a zeolitized tuff exposed to subvolcanic temperatures. R. Soc. Open Sci. 8 (2), 201539.

Mollo, S., Tuccimei, P., Soligo, M., Galli, G., Scarlato, P., 2018. Advancements in understanding the radon signal in volcanic areas: A laboratory approach based on rock physicochemical changes. In: Integrating Disaster Science and Management. Elsevier, pp. 309–328.

Neri, M., Ferrera, E., Giammanco, S., Currenti, G., Cirrincione, R., Patanè, G., Zanon, V., 2016. Soil radon measurements as a potential tracer of tectonic and volcanic activity. Sci. Rep. 6 (1), 24581.

Planinić, J., Radolić, V., Lazanin, Ž., 2001. Temporal variations of radon in soil related to earthquakes. Appl. Radiat. Isot. 55 (2), 267–272.

Rani, P., Ahamed, M.B., Deshmukh, K., 2020. Significantly enhanced electromagnetic interference shielding effectiveness of montmorillonite nanoclay and copper oxide nanoparticles based polyvinylchloride nanocomposites. Polym. Test. 91, 106744.

Sabbarese, C., Ambrosino, F., Chiodini, G., Giudicepietro, F., Macedonio, G., Caliro, S., De Cesare, W., Bianco, F., Pugliese, M., Roca, V., 2020. Continuous radon monitoring during seven years of volcanic unrest at campi flegrei caldera (Italy). Sci. Rep. 10 (1), 9551.

Sakoda, A., Ishimori, Y., Yamaoka, K., 2011. A comprehensive review of radon emanation measurements for mineral, rock, soil, mill tailing and fly ash. Appl. Radiat. Isot. 69 (10), 1422–1435.

Shahbazi-Gahrouei, D., Gholami, M., Setayandeh, S., 2013. A review on natural background radiation. Adv. Biomed. Res. 2 (1), 65.

Singh, K., Scholl, H., Brinkmann, M., Michiel, M.D., Scheel, M., Herminghaus, S., Seemann, R., 2017. The role of local instabilities in fluid invasion into permeable media. Sci. Rep. 7 (1), 444.

Tamburello, G., Caliro, S., Chiodini, G., De Martino, P., Avino, R., Minopoli, C., Carandente, A., Rouwet, D., Aiuppa, A., Costa, A., et al., 2019. Escalating CO2 degassing at the pisciarelli fumarolic system, and implications for the ongoing campi flegrei unrest. J. Volcanol. Geotherm. Res. 384, 151–157.

Terray, L., Gauthier, P.J., Breton, V., Giammanco, S., Sigmarsson, O., Salerno, G., Caltabiano, T., Falvard, A., 2020. Radon activity in volcanic gases of Mt. Etna by passive dosimetry. J. Geophys. Res.: Solid Earth 125 (9), e2019JB019149.

Yokochi, R., Zappala, J.C., Purtschert, R., Mueller, P., 2021. Origin of water masses in floridan aquifer system revealed by 81Kr. Earth Planet. Sci. Lett. 569, 117060.